Validation of the Diffusion Mixture Model for the simulation of bubbly flows and implementation in OpenFOAM

Validation of the Diffusion Mixture Model for the simulation of bubbly flows and implementation in OpenFOAM

Giovanni Tronci[a], Antonio Buffo[a,*], Marco Vanni[a], Daniele L. Marchisio[a]

[a]*Dipartimento di Scienza Applicata e Tecnologia, Istituto di Ingegneria Chimica, Politecnico di Torino, Corso Duca degli Abruzzi 24, 10129 Torino, Italy*

Abstract

In this paper we present the implementation and the validation of the Diffusion Mixture Model as a valuable alternative to other popular models for the simulation of gas-liquid systems. The Diffusion Mixture Model treats the gas-liquid system as if it consists of only one phase: the gas-liquid mixture. The difference between the Diffusion Mixture Model and others lies in the minor simplification made during its development, since a more accurate approach for evaluating the interactions between the different phases is considered. The method is implemented and tested in OpenFOAM, by using as test case a rectangular bubble column. This study shows the effectiveness of the Diffusion Mixture Model which turns out to be accurate, not only in the description of global properties, but also of local quantities. This accuracy comes with a cheaper computational cost as the model solves a smaller number of transport equations, when compared with the two-fluid or the multi-fluid models. Moreover, since this version of the Mixture Models has never been studied in detail, we carried out, during the validation, a thorough analysis on all the simplifications that can be implemented, comparing performance improvements in terms of accuracy and computational costs.

Keywords: Mixture Model, bubble column, multiphase flow, OpenFOAM

1. Introduction

Several industrial applications involve multiphase systems and reactors. Examples of these are heterogeneous bubble columns for the fermentation of biofuels

*Author to whom correspondence should be addressed; mailing address: DISAT - Politecnico di Torino, Corso Duca degli Abruzzi 24, 10129 Torino, Italy; email: antonio.buffo@polito.it; tel. +39 011 0904758; fax: +39 011 0904624

(Gemello et al., 2019, 2018a,b), cyclones (Narasimha et al., 2007), crystallizers (Rielly and Marquis, 2001). In these systems, the interactions between the different phases are significant, as the motion of each phase is influenced by that of the others.

A tool to study, improve and design these devices, is computational fluid dynamics (CFD). CFD is often used as a computational tool to generate digital twins of real cases, especially when combined with deep learning tools (Marcato et al., 2020), giving the advantage of not testing the devices in reality, leading to considerable savings of time and resources. There are several multiphase models that can be used in a CFD simulation and we limit the discussion here to disperse two-phase flows and systems; these are characterized by a continuous primary phase and a secondary disperse phase, comprised of bubbles, droplets or solid particles. The models differ in the type of approach with which the problem is addressed resulting in three categories.

The most accurate and computationally intensive is called direct numerical simulation (DNS) and consists in resolving directly all the interfaces present in the multiphase system (Hager et al., 2013). Among the many methods available it is worth citing the volume-of-fluid method (Hirt and Nichols, 1981; Pham et al., 2020) as well as the discrete element method (Frungieri et al., 2020).

The second category, often referred to as Lagrangian, is based on the idea of neglecting the actual interfaces between the elements of the secondary disperse phase and the primary continuous phase. The elements of the disperse phase are therefore modelled as independent point-particles, each characterized by its own mass, size and velocity (Hermann, 2010; Boccardo et al., 2018b).

The third and last approach, which is the focus of this work, often referred to as Eulerian, is based on the idea of treating the continuous primary phase and the secondary disperse phase as interpenetrating continua. This method has been extensively employed to simulate particle transport in porous media (Boccardo et al., 2019a; Crevacore et al., 2017, 2016; Boccardo et al., 2019b, 2018a; Icardi et al., 2016), bubbly flows in stirred tanks and bubble columns (Buffo et al., 2013a,b, 2012) also under the presence of chemical reactions (Buffo et al., 2017) and boiling flows (Shiea et al., 2019).

DNS is very accurate but very expensive and therefore its use is normally limited to fundamental studies in geometrically simple systems of small size. Similarly, the Lagrangian approach is advantageous if one is interested in studying the individual response of the disperse particles, but becomes computationally demanding in large systems, where a very large number of particles need to be tracked numerically. The third approach is usually the fastest and also the most

used in the industrial sector (Renze et al., 2014) as it is suitable for describing large systems with acceptable computational costs. The price to pay for this cheaper computational costs is the introduction of models to describe the interaction between phases, often in the form of corrections and correlations (Buffo et al., 2016). Readers interested in the details are referred to a recent review (Buffo and Marchisio, 2014). Often these different approaches are coupled together following the multiscale modeling philosophy, which typically requires emphasis on the computational infrastructure and on interoperability as done in other similar areas (Boccardo et al., 2020; Horsch et al., 2020).

There are several models to describe two-phase gas-liquid systems with the Eulerian approach. The Two-Fluid Model (TFM) is based on the solution of one continuity equation and one momentum balance equation for each phase (Ishii and Mishima, 1984). With this approach it is however problematic to deal with the terms representing the interactions between the phases, because of the uncertainty of their predictions and the destabilizing effect they have on the solution process, especially concerning the momentum balance equation. Therefore, proper use of TFM implies a focus on the study of the interfacial terms, and then the formulation of proper constitutive equations (Hibiki and Ishii, 2003b). Notwithstanding these difficulties, the TFM is the most used model for industrial-scale simulations. The TFM was used, for examples, in the investigation of bubble columns (Diaz et al., 2008; Pfleger et al., 1999; Tabib et al., 2007) and nuclear reactor safety (Frank et al., 2008). Furthermore, the TFM has been improved via the coupling with population balance equation (PBE), allowing for the prediction of the bubble size distribution (BSD) (Buffo et al., 2013a; Marchisio and Fox, 2013).

Hence, although the TFM is very popular it is worth exploring alternatives within the context of Eulerian methods. One of this is represented by the Mixture Model (MM) (Manninen and Taivassalo, 1996), based on the simple idea of describing the gas-liquid system as a pseudo single-phase system, called ”mixture phase”, whose properties are intermediate between the different phases that compose the system. In the MM, the typical numerical difficulties that hinder the use of the TFM are reduced, since it is not necessary to instantaneously describe the two separate phases and their transient interactions. In the MM it is assumed that the continuous primary phase and the secondary disperse phase are always in instantaneous equilibrium and the mixture is described with only one momentum balance equation and by algebraic equations that express the relative motion between the phases. Thus the evaluation of the relative velocity between the phases is very important (Hibiki and Ishii, 2003b). The MM has been used in the past (Agarwal and Narayanan, 2018; Icardi et al., 2014, 2013) for the sim-

ulation of gas-liquid and solid-liquid systems but its different variations have not been studied in details.

The MM can, in fact, be divided into three sub-models, based on the simplifications made during its derivation. The easiest, and, at the same time, less accurate version is the Algebraic-Slip Mixture Model (ASMM), implemented in commercial codes such as ANSYS-CFX and ANSYS-Fluent. In the ASMM several important terms that take into account the interaction between phases are neglected, resulting in a valuable alternative only when the disperse phase is very dilute (Brennan, 2003). It is worth mentioning that the model was improved with the implementation of PBE (Chen et al., 2004), resulting in better results. Another version, the most popular of the three, is the Drift-Flux Model (DFM) (Hibiki and Ishii, 2003a), based on the assumptions of constant densities, no interphase exchange and a strictly coupled motion between the phases. For these reasons, the DFM has a limited range of applicability, even if it is more versatile than the ASMM, finding an important use in the description of sedimentation processes (Goda et al., 2003). A version of the DFM is present in the open-source code OpenFOAM in the solver called `driftFluxFoam`.

The last, and more general, version of the model derived from the MM is the Diffusion Mixture Model (DMM). Its applicability is wider since DMM does not have any of the limiting approximations of the other models. To the best of the authors' knowledge, so far the DMM has not been implemented in commercial or open-source CFD codes, unlike ASMM and DFM, and so it has never been tested and analyzed in depth.

Therefore, aiming to find alternatives to the TFM, in this study we investigate the performance of the DMM to simulate gas-liquid bubbly flows. The discussion is here limited to these flows, as bubbles are generally characterized by relatively small Stokes numbers, for which the hypothesis used to derive the DMM governing equations are certainly valid. Due to its characteristics, DMM may be a valid alternative, combining the simplicity and cheap computational cost of the mixture model, with a wider range of applicability. The DMM was implemented for the first time in this work in OpenFOAM 6.0 by modifying the pre-existing solver `driftFluxFoam`. The main focus is on the understanding its performance by comparison with more complex and accurate models, such as the TFM. Secondly, but no less important, particular attention has been paid to the study of the coupling between the velocities of the different phases, focusing on which are the most important terms in these equations. Finally, the last aspect explored in this work for the first time is the analysis of the different simplifications made during the derivation of the model, to understand their impact on the final predictions.

After implementing DMM in OpenFOAM 6.0 the model was validated against some test cases reported in the literature, which refer to bubble columns (Diaz et al., 2008; Pfleger et al., 1999; Buffo et al., 2013a).

The paper is organized as follows. In section 2 the governing equations for the DMM are derived, presented and critically discussed. In section 3 the test cases and the computational details are presented. Then in section 4 the results obtained by running simulations with the DMM are compared with the available experimental data and numerical results obtained with other methods. Finally, in section 5 the conclusions of this work are summarized.

2. Governing equations

The DMM, implemented in OpenFOAM as an incompressible solver, has the capability to model a multi-phase system as a pseudo-single phase system, with properties often described as weighted average between the different phases. In the following section, the governing equations of DMM are presented and discussed. It is useful to point out that in the first part of the discussion a multiphase system constituted of N phases (one of which is continuous and $N-1$ are disperse) is considered. Then the equations are formulated for the simplified case of one continuous phase (i.e. phase 2) and one disperse phase (i.e. phase 1).

2.1. General mixture model equations

The starting point to develop the DMM is to write the continuity and momentum balance equations for a generic phase (indicated with the index k):

$$\frac{\partial}{\partial t}\left(\alpha_k \rho_k\right) + \nabla \cdot \left(\alpha_k \rho_k \mathbf{U}_k\right) = \Gamma_k, \tag{1}$$

$$\frac{\partial}{\partial t}\left(\alpha_k \rho_k \mathbf{U}_k\right) + \nabla \cdot \left(\alpha_k \rho_k \mathbf{U}_k \mathbf{U}_k\right) = \alpha_k \nabla p_k + \nabla \cdot \left[\alpha_k \left(\tau_k + \tau_{Tk}\right)\right] + \alpha_k \rho_k \mathbf{g} + \mathbf{M}_k. \tag{2}$$

The system is turbulent and all the variables in the above equation are ensemble-averaged. The next step is to sum over the N phases that compose the system. For the continuity equation we obtain:

$$\frac{\partial}{\partial t}\sum_{k=1}^{N}\left(\alpha_k \rho_k\right) + \nabla \cdot \sum_{k=1}^{N}\left(\alpha_k \rho_k \mathbf{U}_k\right) = 0, \tag{3}$$

and by defining two new variables: ρ_m, mixture density, and: $\mathbf{U}_\mathrm{m}$, mixture velocity, as follows:

$$\rho_{\mathrm{m}} = \sum_{k=1}^{N} \alpha_k \rho_k \qquad\qquad \mathbf{U}_m = \frac{1}{\rho_{\mathrm{m}}} \sum_{k=1}^{N} \alpha_k \rho_k \mathbf{U}_k, \tag{4}$$

we are able to write the continuity equation for the mixture, which reads as follows:

$$\frac{\partial \rho_{\mathrm{m}}}{\partial t} + \nabla \cdot (\rho_{\mathrm{m}} \mathbf{U}_{\mathrm{m}}) = 0. \tag{5}$$

It is important to notice that the divergence of the mixture velocity is not null: $\nabla \cdot \mathbf{U}_{\mathrm{m}} \neq 0$, since the mixture density is not constant in time nor in space. This fact must be taken into consideration when using the pressuve-velocity algorithm, which, instead, is usually based on the assumption that the divergence of the velocity field is null. However, as shown in section 2.2, the effect is quite small for dilute flows.

Following the same procedure, the momentum equation for the mixture can be obtained and reads as follows:

$$\begin{aligned} \frac{\partial}{\partial t} \sum_{k=1}^{N} (\alpha_k \rho_k \mathbf{U}_k) + \nabla \cdot \sum_{k=1}^{N} (\alpha_k \rho_k \mathbf{U}_k \mathbf{U}_k) = - \sum_{k=1}^{N} (\alpha_k \nabla p_k) + \\ \nabla \cdot \sum_{k=1}^{N} [\alpha_k (\tau_k + \tau_{\mathrm{T}k})] + \sum_{k=1}^{N} (\alpha_k \rho_k \mathbf{g}) + \sum_{k=1}^{N} \mathbf{M}_k. \end{aligned} \tag{6}$$

Now let us introduce a new term, the diffusion velocity $\mathbf{U}_{\mathrm{M}k}$, defined as:

$$\mathbf{U}_{\mathrm{M}k} = \mathbf{U}_k - \mathbf{U}_{\mathrm{m}}. \tag{7}$$

The diffusion velocity is the variable that gives the name to this model. In fact, it is through this velocity that it is possible to relate the properties of the different phases and the mixture, even if the model solves the momentum balance equation only for one phase. Knowing that : $\mathbf{U}_k = \mathbf{U}_{\mathrm{M}k} + \mathbf{U}_{\mathrm{m}}$, it is possible to obtain from Eq. (3) the following relations:

$$\begin{aligned} &\frac{\partial}{\partial t} \sum_{k=1}^{N} (\alpha_k \rho_k) + \nabla \cdot \sum_{k=1}^{N} (\alpha_k \rho_k \mathbf{U}_k) = \\ &\frac{\partial}{\partial t} \sum_{k=1}^{N} (\alpha_k \rho_k) + \nabla \cdot \sum_{k=1}^{N} (\alpha_k \rho_k \mathbf{U}_{Mk} + \alpha_k \rho_k \mathbf{U}_m) = \\ &\frac{\partial \rho_{\mathrm{m}}}{\partial t} + \nabla \cdot (\rho_{\mathrm{m}} \mathbf{U}_{\mathrm{m}}) + \nabla \cdot \sum_{k=1}^{N} (\alpha_k \rho_k \mathbf{U}_{Mk}) = 0, \end{aligned} \tag{8}$$

and by considering Eq. (5), it is easy to obtain:

$$\nabla \cdot \sum_{k=1}^{N} (\alpha_k \rho_k \mathbf{U}_{\mathrm{M}k}) = 0. \tag{9}$$

By using the definition of mixture density and velocity and the result form Eq. (9), we can rewrite the second term of Eq. (6) as follows:

$$\begin{aligned}\nabla \cdot \sum_{k=1}^{N} (\alpha_k \rho_k \mathbf{U}_k \mathbf{U}_k) = \\ \nabla \cdot (\rho_{\mathrm{m}} \mathbf{U}_{\mathrm{m}} \mathbf{U}_{\mathrm{m}}) + \nabla \cdot \sum_{k=1}^{N} (\alpha_k \rho_k \mathbf{U}_{\mathrm{M}k} \mathbf{U}_{\mathrm{M}k}) + 2\nabla \cdot \mathbf{U}_{\mathrm{m}} \sum_{k=1}^{N} (\mathbf{U}_{\mathrm{M}k} \alpha_k \rho_k) = \\ \nabla \cdot (\rho_{\mathrm{m}} \mathbf{U}_{\mathrm{m}} \mathbf{U}_{\mathrm{m}}) + \nabla \cdot \sum_{k=1}^{N} (\alpha_k \rho_k \mathbf{U}_{\mathrm{M}k} \mathbf{U}_{\mathrm{M}k}) .\end{aligned} \tag{10}$$

Eq. (7) defines the diffusion velocity as the difference between the velocity of the generic phase k and the mixture velocity. Summing over all phases and considering that:

$$\sum_{k=1}^{N} \mathbf{M}_k = 0,$$

since interfacial forces eliminate each other, we eventually can write the momentum balance equation for the mixture as follows:

$$\frac{\partial}{\partial t} (\rho_{\mathrm{m}} \mathbf{U}_{\mathrm{m}}) + \nabla \cdot (\rho_{\mathrm{m}} \mathbf{U}_{\mathrm{m}} \mathbf{U}_{\mathrm{m}}) = -\nabla p_{\mathrm{m}} - \nabla \cdot (\tau_{\mathrm{eff}}) + \rho_{\mathrm{m}} \mathbf{g}, \tag{11}$$

where:

$$\tau_{\text{eff}} = \tau_{\text{m}} + \tau_{\text{Tm}} + \tau_{\text{Dm}} \tag{12}$$

$$\tau_{\text{m}} = -\mu_{\text{m}} \sum_{k=1}^{n} \left[\nabla \mathbf{U}_{\text{k}} + (\nabla \mathbf{U}_{\text{k}})^{\text{T}} - \nabla \cdot \frac{2}{3} \mathbf{I} \mathbf{U}_{\text{k}} \right] \tag{13}$$

$$\tau_{\text{Tm}} = -\mu_{\text{Tm}} \sum_{k=1}^{n} \left[\nabla \mathbf{U}_{\text{k}} + (\nabla \mathbf{U}_{\text{k}})^{\text{T}} - \nabla \cdot \frac{2}{3} \mathbf{I} \mathbf{U}_{\text{k}} \right] - \frac{2}{3} \rho_{\text{m}} k_{\text{m}} \mathbf{I}, \tag{14}$$

$$\tau_{\text{Dm}} = -\nabla \cdot \sum_{k=1}^{N} (\alpha_k \rho_k \mathbf{U}_{\text{M}k} \mathbf{U}_{\text{M}k}) \tag{15}$$

$$\mu_{\text{m}} = \sum_{k=1}^{n} \alpha_k \mu_k \tag{16}$$

$$\mu_{\text{Tm}} = \sum_{k=1}^{n} \alpha_k \mu_{\text{T}k}. \tag{17}$$

τ_{m} is the viscous stress related to the mean fluid flow and, consequently, to the molecular mixture viscosity defined in Eq. (16). With τ_{Tm} we indicate the turbulent stress term with the mixture turbulence viscosity defined in Eq. (14). Finally, τ_{Dm} takes into account the stresses generated by the interactions of the two phases. It is important to point out that in Eq. (14), the turbulence is described in terms of the the whole mixture. Another possible approach, when using the TFM, is to consider only the turbulence generated by the continuous phase. The choice of the better approach to describe turbulence together with the attempt of reconciling model simplicity and performance is an essential point for this work, discussed and explained in the next sections.

The last governing equations are the continuity equations for the disperse phases:

$$\frac{\partial}{\partial t} (\alpha_k \rho_k) + \nabla \cdot (\alpha_k \rho_k \mathbf{U}_k) = 0, \tag{18}$$

with $k \in 1 \ldots N-1$ and where the volume fraction for the continuous phase is obtained as the complement to one of the others.

In this work, we consider multiphase systems constituted by a continuous phase (e.g. water) and a secondary disperse phase (e.g. air bubbles). From now on, the disperse phase will be indicated by the index $k = 1$ and the continuous

phase with $k = 2$. Following this notation, the continuity equation for the disperse phase reads as follows:

$$\frac{\partial}{\partial t}\left(\alpha_1 \rho_1\right) + \nabla \cdot \left(\alpha_1 \rho_1 \mathbf{U}_1\right) = 0, \tag{19}$$

and by knowing from Eq. (7) that:

$$\mathbf{U}_1 = \mathbf{U}_\mathrm{m} + \mathbf{U}_{\mathrm{M1}}, \tag{20}$$

and considering constant the two phase densities, it is possible to write the dispersed phase continuity equation only with mixture quantities:

$$\frac{\partial \alpha_1}{\partial t} + \nabla \cdot \left(\alpha_1 \mathbf{U}_\mathrm{m}\right) = -\nabla \cdot \left(\alpha_1 \mathbf{U}_{\mathrm{M1}}\right). \tag{21}$$

In the same way the mixture viscous stress tensor τ and the term τ_{Dm} can be written as follows:

$$\begin{aligned} \tau_\mathrm{m} = \; & \underbrace{-\mu_\mathrm{m}\left[\nabla \mathbf{U}_\mathrm{m} + \left(\nabla \mathbf{U}_\mathrm{m}\right)^\mathrm{T} - \frac{2}{3}\mathbf{I}\left(\nabla \cdot \mathbf{U}_\mathrm{m}\right)\right]}_{\text{viscous stress associated with the mixture}} \\ & -\alpha_1 \mu_1 \left[\nabla \mathbf{U}_{\mathrm{M1}} + \left(\nabla \mathbf{U}_{\mathrm{M1}}\right)^\mathrm{T} - \frac{2}{3}\mathbf{I}\left(\nabla \cdot \mathbf{U}_{\mathrm{M1}}\right)\right] \\ & -\alpha_2 \mu_2 \left[\nabla \mathbf{U}_{\mathrm{M2}} + \left(\nabla \mathbf{U}_{\mathrm{M2}}\right)^\mathrm{T} - \frac{2}{3}\mathbf{I}\left(\nabla \cdot \mathbf{U}_{\mathrm{M2}}\right)\right] \end{aligned} \tag{22}$$

and as follows:

$$\tau_{\mathrm{Dm}} = -\nabla \cdot \left(\alpha_1 \rho_1 \mathbf{U}_{\mathrm{M1}} \mathbf{U}_{\mathrm{M1}} + \alpha_2 \rho_2 \mathbf{U}_{\mathrm{M2}} \mathbf{U}_{\mathrm{M2}}\right). \tag{23}$$

Accordingly to Manninen and Taivassalo (1996) some of the terms appearing in Eq. (22) can be neglected. In fact, in dilute systems the first term, accounting for the viscous stress associated to the mixture, is often more important than the others, that take into account the viscous stress caused by the relative motion between the phases. For this reason only the first term is usually considered in dilute systems. However, the effect of this approximation has never been assessed in an actual simulation and since our objective is to develop and test a methodology of general applicability, it is worth further investigating this point. For this reason, we will test the code with and without the diffusion velocity viscous stresses.

All the equations obtained depend on the diffusion velocities, so it is necessary to find a relationship to calculate this variable. To do this, we introduce the relative

velocity, obtained as the difference between the velocity of the disperse and the continuous phase:

$$\mathbf{U}_\mathrm{r} = \mathbf{U}_1 - \mathbf{U}_2. \tag{24}$$

From this definition and from Eq. (4) we obtain the following relationship between $\mathbf{U}_\mathrm{r}$ and the diffusive velocities:

$$\mathbf{U}_{\mathrm{M1}} = \mathbf{U}_1 - \mathbf{U}_\mathrm{m} = \frac{\alpha_2\rho_2}{\rho_\mathrm{m}}\mathbf{U}_\mathrm{r} = \left(1 - \frac{\alpha_1\rho_1}{\rho_\mathrm{m}}\right)\mathbf{U}_\mathrm{r}, \tag{25}$$

$$\mathbf{U}_{\mathrm{M2}} = \mathbf{U}_2 - \mathbf{U}_\mathrm{m} = -\frac{\alpha_1\rho_1}{\rho_\mathrm{m}}\mathbf{U}_\mathrm{r}. \tag{26}$$

It will be discussed later on how to close these expressions by finding a relationship for $\mathbf{U}_\mathrm{r}$.

It is important now to derive another quantity, essential for highlighting a further simplification of the model. Summing together the continuity equation for the two phases in the form of Eq. (19) we obtain:

$$\frac{\partial}{\partial t}(\alpha_1 + \alpha_2) + \nabla \cdot (\alpha_1\mathbf{U}_1 + \alpha_2\mathbf{U}_2) = 0. \tag{27}$$

The first term is null since $\alpha_1 + \alpha_2$ is constant and equal to one . Consequently also the second terms is null. This term in particular represents the mixture volumetric flux and can be written as follows:

$$\nabla \cdot \mathbf{j}_\mathrm{m} = \nabla \cdot (\alpha_1\mathbf{U}_1 + \alpha_2\mathbf{U}_2) = 0. \tag{28}$$

The reader should notice that there is a difference between $\mathbf{j}_\mathrm{m}$ and $\mathbf{U}_\mathrm{m}$, since, as previously mentioned, the divergence of $\mathbf{U}_\mathrm{m}$ is not null instead. This aspect will be further clarified in the following section.

2.2. Relationship between $\mathbf{U_m}$ *and* $\mathbf{j}_\mathrm{m}$

As mentioned before, the mass flux $\nabla \cdot \mathbf{U_m}$ is not zero, and this must be taken into account when developing the solution algorithm. On the other hand, as just explained, the mixture volumetric flux, $\nabla \cdot \mathbf{j}_\mathrm{m}$, is always zero, as a result of Eq. (27). As demonstrated by Ungarish (1993) there is a relationship between $\mathbf{U_m}$ and $\mathbf{j}_\mathrm{m}$ which reads as follows:

$$\mathbf{U_m} = \mathbf{j}_\mathrm{m} + \alpha_1\alpha_2\frac{(\rho_1 - \rho_2)}{\rho_\mathrm{m}}\mathbf{U_r}. \tag{29}$$

By applying the divergence operator on both sides, the following expression can be obtained:

$$\nabla \cdot \mathbf{U_m} = \nabla \cdot \left(\alpha_1 \alpha_2 \frac{(\rho_1 - \rho_2)}{\rho_\mathrm{m}} \mathbf{U_r} \right). \tag{30}$$

This relationship shows that the divergence of the mixture velocity is not null, especially where the mixture has a significant content of the dispersed phase. This term can be neglected when α_1 and α_2 are very low, whereas it becomes important in regimes where the volume of continuous and dispersed phases have similar values. This is, for instance, the case of the phase inversion zone close to the liquid free surface. Since we are not interested in the detailed simulation of this portion of the domain and being the gas hold-up quite small in the investigated cases, we decided to fix $\nabla \cdot \mathbf{U}_m = 0$ in this work. However in principle, this term should be considered in the pressure-velocity coupling algorithm.

2.3. Closure for the relative velocity

It is now necessary to find a relationship to compute the relative velocity $\mathbf{U}_\mathrm{r} = (\mathbf{U}_1 - \mathbf{U}_2)$, which is needed to evaluate the diffusion velocities and hence to close the model. Such relationship can be algebraic (i.e, Algebraic Slip Model) or differential according to the level of detail aimed for. In this work we will show how to derive a full differential model to calculate $\mathbf{U}_r$ and then we propose and test some possible simplifications.

The starting point is the momentum balance for the disperse phase, which reads as follows:

$$\alpha_1 \rho_1 \frac{\partial \mathbf{U}_1}{\partial t} + \alpha_1 \rho_1 \left(\mathbf{U}_1 \cdot \nabla \right) \mathbf{U}_1 = -\alpha_1 \nabla p_1 + \nabla \cdot \left[\alpha_1 \left(\tau_1 + \tau_{\mathrm{T}1} \right) \right] + \alpha_1 \rho_1 \mathbf{g} + \mathbf{M}_1, \tag{31}$$

where $\mathbf{M}_1$ is the interfacial force per unit volume, which includes drag, lift, virtual mass, etc. exchanged between the bubbles and the surrounding continuous phase. The reader should note that Eq. (31) is valid only if

$$\frac{\partial \rho_1 \alpha_1}{\partial t} + \nabla \cdot (\rho_1 \alpha_1 \mathbf{U}_1) = 0,$$

in other words when there is no mass transfer between the phases. Considering that the mixture phase and the disperse phase share the same pressure ($\nabla p_1 = \nabla p_\mathrm{m}$), it is possible to substitute Eq. (20) into Eq. (31), leaving only the interface momentum term on the left-hand side, obtaining the following relationship :

$$\mathbf{M}_1 = \alpha_1 \left[\underbrace{\rho_1 \frac{\partial \mathbf{U}_1}{\partial t}}_{\mathcal{A}} - \rho_\mathrm{m} \frac{\partial \mathbf{U}_\mathrm{m}}{\partial t} \right] + \alpha_1 \left[\underbrace{\rho_1 \left(\mathbf{U}_1 \cdot \nabla\right) \mathbf{U}_1}_{\mathcal{A}} - \rho_\mathrm{m} \left(\mathbf{U}_\mathrm{m} \cdot \nabla\right) \mathbf{U}_\mathrm{m} \right] - \nabla \cdot \left[\alpha_1 \left(\underbrace{\tau_1}_{\mathcal{B}} + \underbrace{\tau_{\mathrm{T}1}}_{\mathrm{C}} \right) \right] + \alpha_1 \nabla \cdot \left(\underbrace{\tau_\mathrm{m} + \tau_{\mathrm{D}m}}_{\mathcal{B}} + \underbrace{\tau_{\mathrm{T}m}}_{C} \right) - \alpha_1 \left(\rho_1 - \rho_\mathrm{m}\right) \mathbf{g} \quad (32)$$

Since Eq. (32) contains many terms, let us speculate about possible simplifications, as done in the work of Manninen and Taivassalo (1996). First of all we have to rewrite and analyze the term $\mathcal{A}$ as a function of mixture quantities. With the definition of diffusion velocity reported in Eq. (7) it is possible to decompose these terms in three parts, as follows:

$$\alpha_1 \rho_1 \left(\frac{\partial \mathbf{U}_1}{\partial t} + \mathbf{U}_1 \cdot \nabla \mathbf{U}_1 \right) = \underbrace{\alpha_1 \rho_1 \left(\frac{\partial \mathbf{U}_{\mathrm{M}1}}{\partial t} + \mathbf{U}_{\mathrm{M}1} \cdot \nabla \mathbf{U}_{\mathrm{M}1} \right)}_{\mathcal{A}_1} + \underbrace{\alpha_1 \rho_1 \left(\mathbf{U}_\mathrm{m} \cdot \nabla \mathbf{U}_{\mathrm{M}1} + \mathbf{U}_{\mathrm{M}1} \cdot \nabla \mathbf{U}_\mathrm{m} \right)}_{\mathcal{A}_2} + \underbrace{\alpha_1 \rho_1 \left(\frac{\partial \mathbf{U}_\mathrm{m}}{\partial t} + \mathbf{U}_\mathrm{m} \cdot \nabla \mathbf{U}_\mathrm{m} \right)}_{\mathcal{A}_3} \quad (33)$$

By performing here the approximation of local equilibrium, $\mathcal{A}_1$ and $\mathcal{A}_2$ can be neglected if the bubbles accelerate quickly to terminal velocity. $\mathcal{A}_3$ will instead be kept as it is never negligible. The viscous and the diffusion stresses ($\mathcal{B}$ terms) can be also neglected, especially when convection of momentum is prevailing over diffusion. The system we have to model is mildly turbulent, so also the turbulent stress tensors (C terms) can be neglected in this momentum balance of the dispersed phase (but not in the overall model). By neglecting all these terms Eq. (32) becomes:

$$\mathbf{M}_1 = +\alpha_1 \left(\rho_1 - \rho_\mathrm{m}\right) \frac{\partial \mathbf{U}_\mathrm{m}}{\partial t} + \alpha_1 \left(\rho_1 - \rho_\mathrm{m}\right) \left(\mathbf{U}_\mathrm{m} \cdot \nabla\right) \mathbf{U}_\mathrm{m} - \alpha_1 \left(\rho_1 - \rho_\mathrm{m}\right) \mathbf{g} \quad (34)$$

The last step is the substitution of $\mathbf{M_1}$ with the expression of all the relative interfacial forces, which are usually function of the relative velocity. By considering only the drag force, which is normally the most important interfacial interaction, $\mathbf{M_1}$ can be written as:

$$\mathbf{M}_1 = -\alpha_1 \frac{3}{4} \frac{\rho_2 C_\mathrm{D}}{d} |\mathbf{U}_\mathrm{r}| \mathbf{U}_\mathrm{r}, \tag{35}$$

where $\mathbf{M}_1$ has the unit of a force per unit volume, d is the bubble diameter and C_D is the drag coefficient.

The drag-force coefficient C_D is computed with the correlation developed by Tomiyama et al. (2002) for contaminated fluids:

$$C_\mathrm{D} = \max\left[\frac{24}{\mathrm{Re_p}}\left(1 + 0.15\mathrm{Re_p}^{0.687}\right), \frac{8}{3}\frac{\mathrm{Eo}}{\mathrm{Eo}+4}\right], \tag{36}$$

$$\mathrm{Re_p} = \frac{\rho_2 \mathbf{U}_\mathrm{r} \mathrm{d}}{\mu_2}, \tag{37}$$

$$\mathrm{Eo} = \frac{(\rho_2 - \rho_1)\, \mathbf{g} \mathrm{d}^2}{\sigma}, \tag{38}$$

where σ is the surface tension, Re is the bubble Reynolds numbers and Eo is the Eötvos number.

Now substituting Eq. (35) in Eq. (34) the following equation can be derived:

$$|\mathbf{U}_\mathrm{r}|\mathbf{U}_\mathrm{r} = -\frac{4}{3}\frac{d}{\rho_2 C_\mathrm{D}} (\rho_1 - \rho_m) \left[\frac{\partial \mathbf{U}_\mathrm{m}}{\partial t} - (\mathbf{U}_\mathrm{m} \nabla \cdot \mathbf{U}_\mathrm{m}) + \mathbf{g}\right]. \tag{39}$$

It is important to notice that the above equation must be solved with an iterative method since the drag-force coefficient C_D depends on the relative velocity $\mathbf{U}_\mathrm{r}$ in a non linear manner. In this study, we chose the iterative Newton-Raphson (Press et al., 2007).

If, instead, no simplification is performed on the momentum equation of the disperse phase and, consequently, we substitute Eq. (35) in Eq. (32) the result is:

$$\begin{aligned} |\mathbf{U}_\mathrm{r}|\mathbf{U}_\mathrm{r} = \frac{4}{3}\frac{d}{\rho_2 C_\mathrm{D}} \Bigg\{ & \alpha_1 \left[\rho_1 \frac{\partial \mathbf{U}_\mathrm{M1}}{\partial t} + (\rho_1 - \rho_\mathrm{m}) \frac{\partial \mathbf{U}_\mathrm{m}}{\partial t}\right] \\ & + \alpha_1 \left[\rho_1 (\mathbf{U}_1 \cdot \nabla) \mathbf{U}_1 - \rho_\mathrm{m} (\mathbf{U}_\mathrm{m} \cdot \nabla) \mathbf{U}_\mathrm{m}\right] - \nabla \cdot \left[\alpha_1 (\tau_1 + \tau_{\mathrm{T}1})\right] \\ & + \alpha_1 \nabla \cdot (\tau_\mathrm{m} + \tau_{\mathrm{Tm}} + \tau_{\mathrm{Dm}}) - \alpha_1 (\rho_1 - \rho_\mathrm{m}) \mathbf{g} \Bigg\}. \end{aligned} \tag{40}$$

This equation contains all the terms previously neglected. Due to the fact that both $\mathbf{U}_{\mathrm{M1}}$ and $\mathbf{U}_1$ depend on $\mathbf{U}_\mathrm{r}$, such equation it is not only non-linear but also differential. To better understand when and if these approximations are valid, in this work we test the DMM with both formulations for the calculation of the relative velocity in order to understand the importance of all the simplifications.

2.4. Turbulence modelling

The k-ϵ model is used here to compute the turbulent viscosity and the turbulent stress tensor. Two approaches are available. The first one, computes turbulence by using the continuous phase velocity to solve the k-ϵ equations:

$$\begin{aligned}
&\frac{\partial \alpha_2 \rho_2 k}{\partial t} + \nabla \cdot (\alpha \rho_2 \mathbf{U}_2 k) - \nabla \cdot \left(\alpha_2 \frac{\mu_{\mathrm{t2}}}{\sigma_k} \nabla k \right) = \rho_2 \alpha_2 \left(\mathrm{G} - k \right), \\
&\frac{\partial \alpha_2 \rho_2 \epsilon}{\partial t} + \nabla \cdot (\alpha_2 \rho_2 \mathbf{U}_2 \epsilon) - \nabla \cdot \left(\alpha_2 \frac{\mu_{\mathrm{t2}}}{\sigma_\epsilon} \nabla \epsilon \right) = \rho_2 \alpha_2 \left(\mathrm{C}_{\epsilon,1} \frac{\epsilon}{k} \mathrm{G} - \mathrm{C}_{\epsilon,2} \frac{\epsilon^2}{k} \right).
\end{aligned} \tag{41}$$

This is a good approximation for dilute systems since the turbulent stresses generated by the continuous phase are usually more important than those of the disperse phase. This approach is often used in TFM, however, differently from the TFM, in the MM $\mathbf{U}_2$ is not a transported quantity, since it is not solved via a balance equation, leading to potential inaccuracies. Hence, the second approach, being based on the resolution of the k-ϵ equations with the mixture velocity $\mathbf{U}_\mathrm{m}$, seems to be more consistent with the MM, which relies on the solution of the mixture velocity field:

$$\begin{aligned}
&\frac{\partial \rho_\mathrm{m} k}{\partial t} + \nabla \cdot (\alpha \rho_\mathrm{m} \mathbf{U}_m k) - \nabla \cdot \left(\frac{\mu_{\mathrm{tm}}}{\sigma_k} \nabla k \right) = \rho_\mathrm{m} \left(\mathrm{G} - k \right), \\
&\frac{\partial \rho_\mathrm{m} \epsilon}{\partial t} + \nabla \cdot (\rho_\mathrm{m} \mathbf{U}_\mathrm{m} \epsilon) - \nabla \cdot \left(\frac{\mu_{\mathrm{tm}}}{\sigma_\epsilon} \nabla \epsilon \right) = \rho_\mathrm{m} \left(\mathrm{C}_{\epsilon,1} \frac{\epsilon}{k} \mathrm{G} - \mathrm{C}_{\epsilon,2} \frac{\epsilon^2}{k} \right).
\end{aligned} \tag{42}$$

Simulations in this work will be performed by considering both the continuous phase velocity (approach 1) and the mixture velocity (approach 2) for the solution of the k-ϵ governing equations. It is interesting to highlight that the second approach is faster, since it is directly formulated in terms of $\mathbf{U}_\mathrm{m}$, while the continuous phase velocity, necessary for the first approach, is a variable not directly computed in the MM, leading therefore to higher computational costs.

2.5. Solver description

In Fig. 1, a block diagram representing the algorithm employed by the solver is reported. Initially, we define the initial and boundary conditions,and compute densities and viscosities. In the second step, $\mathbf{U_r}$ is calculated by solving Eq. (39) with the Newton-Raphson method, since the drag-force coefficient C_D depends on $\mathbf{U_r}$. By knowing $\mathbf{U_r}$ it is now possible to compute τ_Dm from Eq. (23), the term that takes into account the interaction between the different phases. The disperse phase volume fraction α_1 is evaluated by solving Eq. (21), whereas Eq. (11) is used to compute the predicted $\mathbf{U_m}$. Then the pressure velocity algorithm runs a number of times sufficient to converge to a solution. Finally, with the updated mixture velocity the time is advanced and the simulation continues. All this procedure is repeated until the final timestep is reached. These steps are present in all the different models tested. The difference between the simplified model with all the possible simplifications and the others is that in the case we want to consider all the terms, and so compute $\mathbf{U}_1$ and $\mathbf{U}_2$, it is necessary to repeat the computation of $\mathbf{U}_{21}$ until these three quantities converge.

3. Test cases and computational details

The test cases are all based on the bubble column experimentally investigated by Diaz et al. (2008). The column has dimensions 0.2 m $\times$ 0.04 m $\times$ 1.8 m high and is filled with tap water (the continuous phase) up to 0.45 m at atmospheric pressure and temperature. The air is injected from the bottom with a sparger located in the centre by eight holes of 1 mm in diameter. The density and viscosity of the fluids are taken at the temperature of 20° C . Air density is 1.255 $^{\mathrm{kg}}/_{\mathrm{m}^3}$ and its viscosity is 1.813×10^{-5} Pa s, while water density is 998.2 $^{\mathrm{kg}}/_{\mathrm{m}^3}$ and its viscosity is 1.0×10^{-3} Pa s. Simulation results were compared with experimental data of Diaz et al. (2008) and TFM simulation results of Buffo et al. (2013a) for two global quantities: the gas hold-up in the column and the Plume Oscillation Period (POP). DMM simulations were carried out on a non-uniform hexahedral grid made of $32 \times 11 \times 65$ cells (Fig 2). The choice of this grid is motivated by the results obtained by Buffo et al. (2013a), since this grid has a degree of refinement sufficient to capture the dynamics of the problem.

The sparger was modelled as rectangularly shaped with the same area as the real eight holes. Air is injected imposing an inlet volume fraction equal to unity with a velocity computed as follows:

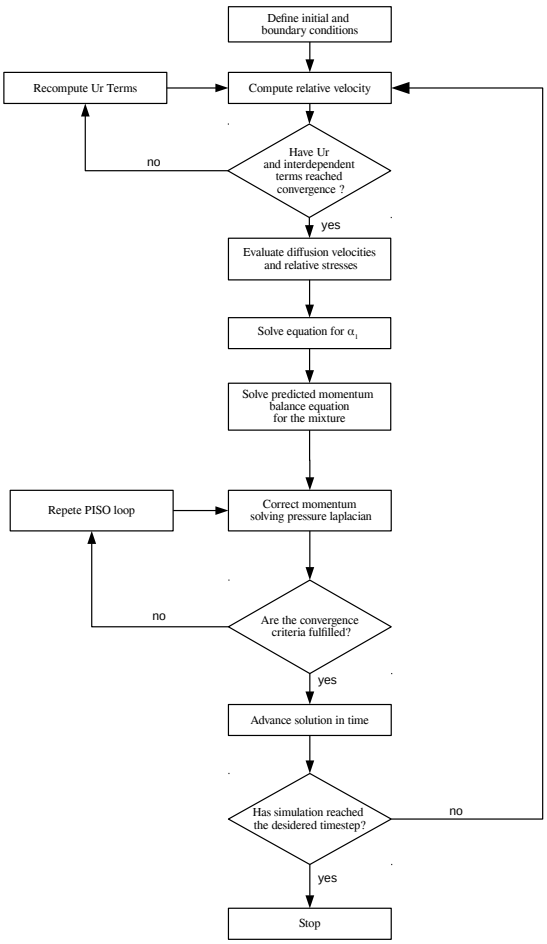

Figure 1: Block diagram of the DMM algorithm implemented in OpenFOAM.

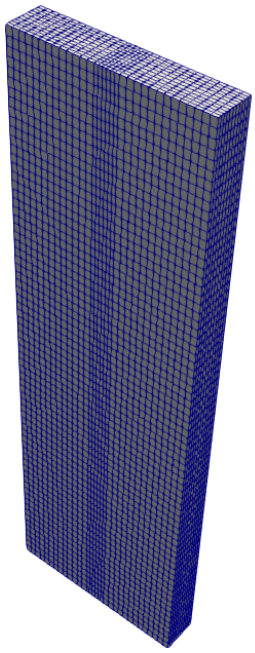

Figure 2: Snapshot of the mesh employed in the DMM simulations.

$$\text{Inlet Gas Velocity} = \frac{\text{Gas Flow Rate}}{\text{Modeled Sparger Area x Gas Volume Fraction}} \tag{43}$$

This and the other boundary conditions are summarized in Tab. 1.

With the purpose of comparing the DMM results with Diaz et al. (2008) and Buffo et al. (2013a), five different superficial velocities were prescribed and investigated. In all the cases, the bubbles diameter is kept constant during all the simulations, differently from Buffo et al. (2013a) that coupled the TFM with a population balance. This difference should be considered when the two methods are compared.

At the beginning of this work, only the liquid part of the bubble column was considered, with the aim of saving computational time. However, this approach was proven to be unsuccessful since the bubble plume moved in a non-physical way: this behavior was caused by the computation of k and ϵ at the gas-liquid interface where their values were imposed as boundary conditions instead of being calculated. For this reason, the simulations were then initialized by dividing the domain into two zones, forcing the DMM to calculate also the gas-liquid interface.

Table 1: Numerical schemes and boundary conditions adopted in the DMM simulations

Variable	**Scheme**	**Inlet**	**Outlet**	**Wall**
Gas vol. frac.	Lim. 2^{nd} ord. upwind	1.0	Zero grad.	Zero grad.
Mixture velocity	2^{nd} ord. upwind	Depends on flow rate	Zero grad. with backflow	No-slip
Pressure	2^{nd} ord. upwind	fixed flux	1 bar	fixed flux
k	2^{nd} ord. upwind	Based on turbulence intensity equal to 5% and length scale equal to the hole diameter	Zero grad.	Zero grad.
ϵ	2^{nd} ord. upwind		Zero grad.	Zero grad.

The bottom region has a zero gas volume fraction and the top has a gas volume fraction of one. This sharp discontinuity leads to numerical instabilities in the air zone on the top. These numerical instabilities are caused by the calculation of the relative velocity $\mathbf{U}_r$, which is coupled in each time-step and for each cell. In this sense, it is worth remarking that Eq. (39) and Eq. (40) are defined only where the gas is dispersed, namely in zone below the liquid free surface. To avoid the numerical instabilities, $\mathbf{U}_r$ is not computed when $\alpha_1 = 0$, but it is fixed to a small predetermined value, equal to 10^{-8}. This numerical trick is consistent with reality, since $\mathbf{U}_m = \mathbf{U}_1$ in the upper part of the domain where there is no liquid. In this way, DMM is able to switch robustly from mixtures to pure phases. It is important to notice that this problem does not arise in the a pure liquid phase zone, since $\mathbf{U}_r$ vanishes when $\alpha_1 = 0$ according with Eq. (39) (since $\rho_1 = \rho_m$) and Eq. (40).

Another test case, based on the bubble column investigated by Pfleger et al. (1999) was also considered. This column is slightly different from the one investigated by Diaz et al. (2008), since the width is 0.05 m instead of 0.04 m. The aim of this test case is to calculate the vertical velocity profiles along the horizontal axis at three different heights (0.13 m - 0.25 m - 0.37 m) and compare them with the results obtained by TFM and with experiments. This test case will show the capability of the model to predict not only global properties as gas hold-up and POP, but also local properties as the local vertical velocity profile.

In order to compare possible different implementations, various ways to compute turbulent quantities will be explored in this work. Now for simplicity, a nomenclature is introduced to identify better the tested models according to the adopted turbulence model and the simplifications made. The label "1" refers to the approach where turbulence is transported only by the continuous phase, while

the label "2" to simulations in which the turbulence is transported by the mixture (see paragraph 2.4). Moreover, to indicate the various simplifications made four different suffixes are employed: *A* if all the simplifications presented in Sections 2.1 and 2.3 are employed, *B* if none of them are made, *C* if only the simplification in Section 2.1 are employed and *D* if those in Section 2.3 are made. Table 3 summarizes the situation, reporting approximations and terms considered.

Suffixes	Approximations and term considered
A	$\tau_{\mathrm{m}} = -\mu_{\mathrm{m}}\left[\nabla\mathbf{U}_{\mathrm{m}} + (\nabla\mathbf{U}_{\mathrm{m}})^{\mathrm{T}} - \frac{2}{3}\mathbf{I}\left(\nabla\cdot\mathbf{U}_{\mathrm{m}}\right)\right]$ $\mathbf{U}_{\mathrm{r}}^{2} = -\frac{4}{3}\frac{d}{\rho_2 C_{\mathrm{D}}}\left(\rho_1 - \rho_m\right)\left[\frac{\partial\mathbf{U}_{\mathrm{m}}}{\partial t} - \left(\mathbf{U}_{\mathrm{m}}\nabla\cdot\mathbf{U}_{\mathrm{m}}\right) + \mathbf{g}\right]$
B	$\tau_{\mathrm{m}} = -\mu_{\mathrm{m}}\left[\nabla\mathbf{U}_{\mathrm{m}} + (\nabla\mathbf{U}_{\mathrm{m}})^{\mathrm{T}} - \frac{2}{3}\mathbf{I}\left(\nabla\cdot\mathbf{U}_{\mathrm{m}}\right)\right]$ $-\alpha_1\mu_1\left[\nabla\mathbf{U}_1 + (\nabla\mathbf{U}_1)^{\mathrm{T}} - \frac{2}{3}\mathbf{I}\left(\nabla\cdot\mathbf{U}_1\right)\right]$ $-\alpha_2\mu_2\left[\nabla\mathbf{U}_2 + (\nabla\mathbf{U}_2)^{\mathrm{T}} - \frac{2}{3}\mathbf{I}\left(\nabla\cdot\mathbf{U}_2\right)\right]$ $\mathbf{U}_{\mathrm{r}}^{2} = \frac{4}{3}\frac{d}{\rho_2 C_{\mathrm{D}}}\Big\{\alpha_1\left[\rho_1\frac{\partial\mathbf{U}_{\mathrm{M1}}}{\partial t} + \left(\rho_1 - \rho_{\mathrm{m}}\right)\frac{\partial\mathbf{U}_{\mathrm{m}}}{\partial t}\right] + \alpha_1\left[\rho_1\left(\mathbf{U}_1\cdot\nabla\right)\mathbf{U}_1 - \rho_{\mathrm{m}}\left(\mathbf{U}_{\mathrm{m}}\cdot\nabla\right)\mathbf{U}_{\mathrm{m}}\right]$ $-\nabla\cdot\left[\alpha_1\left(\tau_1 + \tau_{\mathrm{T1}}\right)\right] + \alpha_1\nabla\cdot\left(\tau_{\mathrm{m}} + \tau_{\mathrm{Tm}} + \tau_{\mathrm{Dm}}\right) - \alpha_1\left(\rho_1 - \rho_{\mathrm{m}}\right)\mathbf{g}\Big\}$
C	$\tau_{\mathrm{m}} = -\mu_{\mathrm{m}}\left[\nabla\mathbf{U}_{\mathrm{m}} + (\nabla\mathbf{U}_{\mathrm{m}})^{\mathrm{T}} - \frac{2}{3}\mathbf{I}\left(\nabla\cdot\mathbf{U}_{\mathrm{m}}\right)\right]$ $-\alpha_1\mu_1\left[\nabla\mathbf{U}_1 + (\nabla\mathbf{U}_1)^{\mathrm{T}} - \frac{2}{3}\mathbf{I}\left(\nabla\cdot\mathbf{U}_1\right)\right]$ $-\alpha_2\mu_2\left[\nabla\mathbf{U}_2 + (\nabla\mathbf{U}_2)^{\mathrm{T}} - \frac{2}{3}\mathbf{I}\left(\nabla\cdot\mathbf{U}_2\right)\right]$ $\mathbf{U}_{\mathrm{r}}^{2} = -\frac{4}{3}\frac{d}{\rho_2 C_{\mathrm{D}}}\left(\rho_1 - \rho_m\right)\left[\frac{\partial\mathbf{U}_{\mathrm{m}}}{\partial t} - \left(\mathbf{U}_{\mathrm{m}}\nabla\cdot\mathbf{U}_{\mathrm{m}}\right) + \mathbf{g}\right]$
D	$\tau_{\mathrm{m}} = -\mu_{\mathrm{m}}\left[\nabla\mathbf{U}_{\mathrm{m}} + (\nabla\mathbf{U}_{\mathrm{m}})^{\mathrm{T}} - \frac{2}{3}\mathbf{I}\left(\nabla\cdot\mathbf{U}_{\mathrm{m}}\right)\right]$ $\mathbf{U}_{\mathrm{r}}^{2} = \frac{4}{3}\frac{d}{\rho_2 C_{\mathrm{D}}}\Big\{\alpha_1\left[\rho_1\frac{\partial\mathbf{U}_{\mathrm{M1}}}{\partial t} + \left(\rho_1 - \rho_{\mathrm{m}}\right)\frac{\partial\mathbf{U}_{\mathrm{m}}}{\partial t}\right] + \alpha_1\left[\rho_1\left(\mathbf{U}_1\cdot\nabla\right)\mathbf{U}_1 - \rho_{\mathrm{m}}\left(\mathbf{U}_{\mathrm{m}}\cdot\nabla\right)\mathbf{U}_{\mathrm{m}}\right]$ $-\nabla\cdot\left[\alpha_1\left(\tau_1 + \tau_{\mathrm{T1}}\right)\right] + \alpha_1\nabla\cdot\left(\tau_{\mathrm{m}} + \tau_{\mathrm{Tm}} + \tau_{\mathrm{Dm}}\right) - \alpha_1\left(\rho_1 - \rho_{\mathrm{m}}\right)\mathbf{g}\Big\}$

Table 2: Summary of the different versions of the DMM investigated. Label **A** represents the model with all the simplification proposed by Manninen and Taivassalo (1996). Label **B** represents the model with no simplifications. Label **C** represents the model employing the simplified Eq. 39 only. Label **D** refers to the model employing the simplified version of Eq. 22.

4. Results and discussion

As previously mentioned, our model predictions were tested by comparing the results obtained with the experimental measurements of Diaz et al. (2008), and the TFM predictions of Buffo et al. (2013a). An in-depth analysis on the different simplifications suggested by Manninen and Taivassalo (1996) has been conducted, pointing out the relation between model accuracy and computational cost.

0_____ DANIELE'S NOTE _____0
What DMM is this one reported in the Figure A, B, C or D?Antonio: I think is 2A, but I am not sure. Giovanni should know the answer

The first confirmation of the good performance of the model can be obtained by observing Fig. 3, where the snapshot of the results obtained by experiments, TFM and DMM are represented and compared for three different superficial velocities. The DMM returns results similar to those obtained by TFM and by the experiments, proving, qualitatively, that the model is capable of describing the typical features of this gas-liquid flow, such as the larger gas concentration in the centre of the column, that leads to the formation of an oscillating bubble plume and the entrapment of bubbles on the sides of the column below the interface at high superficial velocities.

Another qualitative comparison is carried out in Fig. 4, where the central plane snapshots of the gas volume fraction for the investigated eight different DMM implementations taken for the same operating condition (superficial gas velocity equal to 11.9 mm/s) and time step are reported. As it can be seen from the figure, there is no substantial difference between the different implementations: the expected oscillating bubble plume is formed in all the cases with similar features. However it is worth noticing that there are no identical contour plots, meaning that the position and the shape of the plume are different due to the effect of the different models considered. The same behavior has been also observed for all the five operating conditions investigated, thus motivating the following quantitative analysis.

As anticipated in Section 3, the bubbles are considered monodispersed. Their size is taken from the experimental data of Diaz et al. (2008) and it is indicated in Tab. 3. The data is obtained by simulating the process for 300 s and sampling the quasi-periodic behavior that is established after the transient, ranging from 40 s to

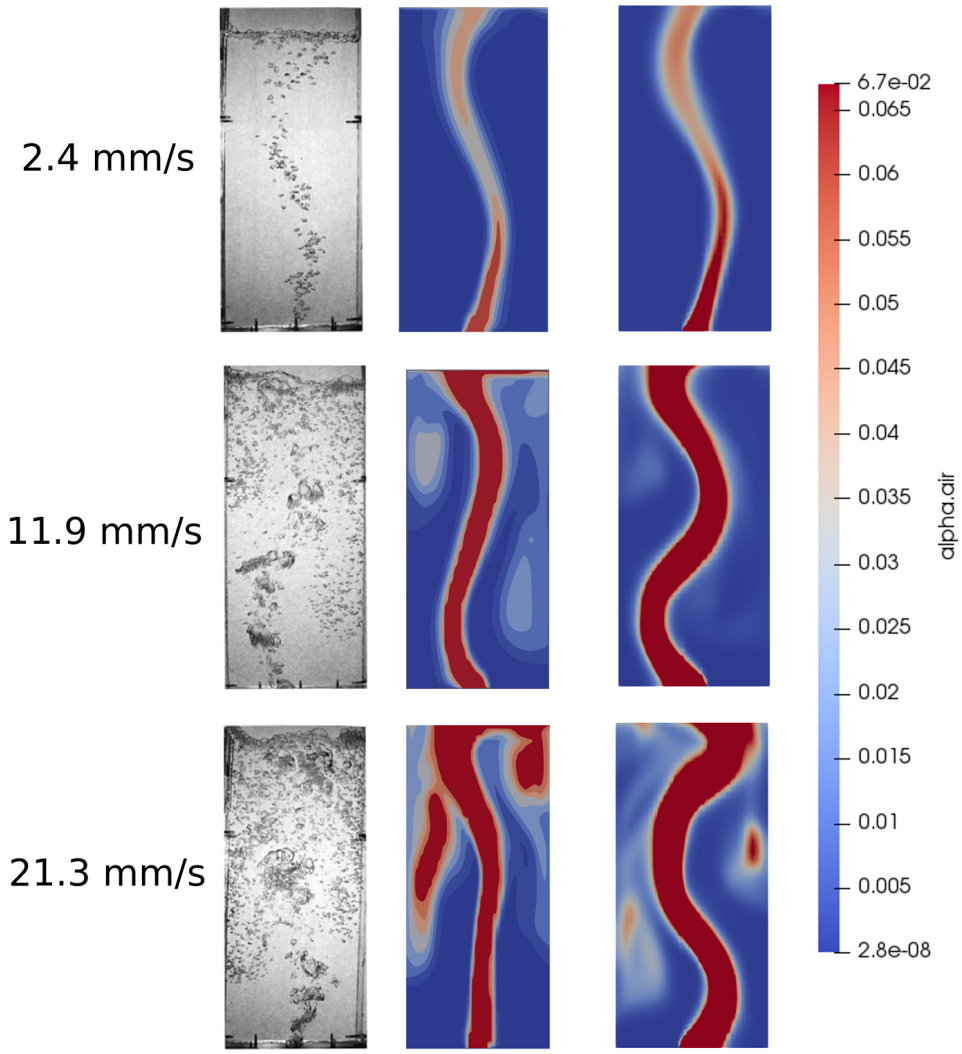

Figure 3: Instantaneous gas distributions from: experiments (left column),TFM (central column), DMM (right column) for three different superficial velocities (2.4 mm/s, 11.9 mm/s and 21.3 mm/s). The quantity plotted is the local gas volume fraction.

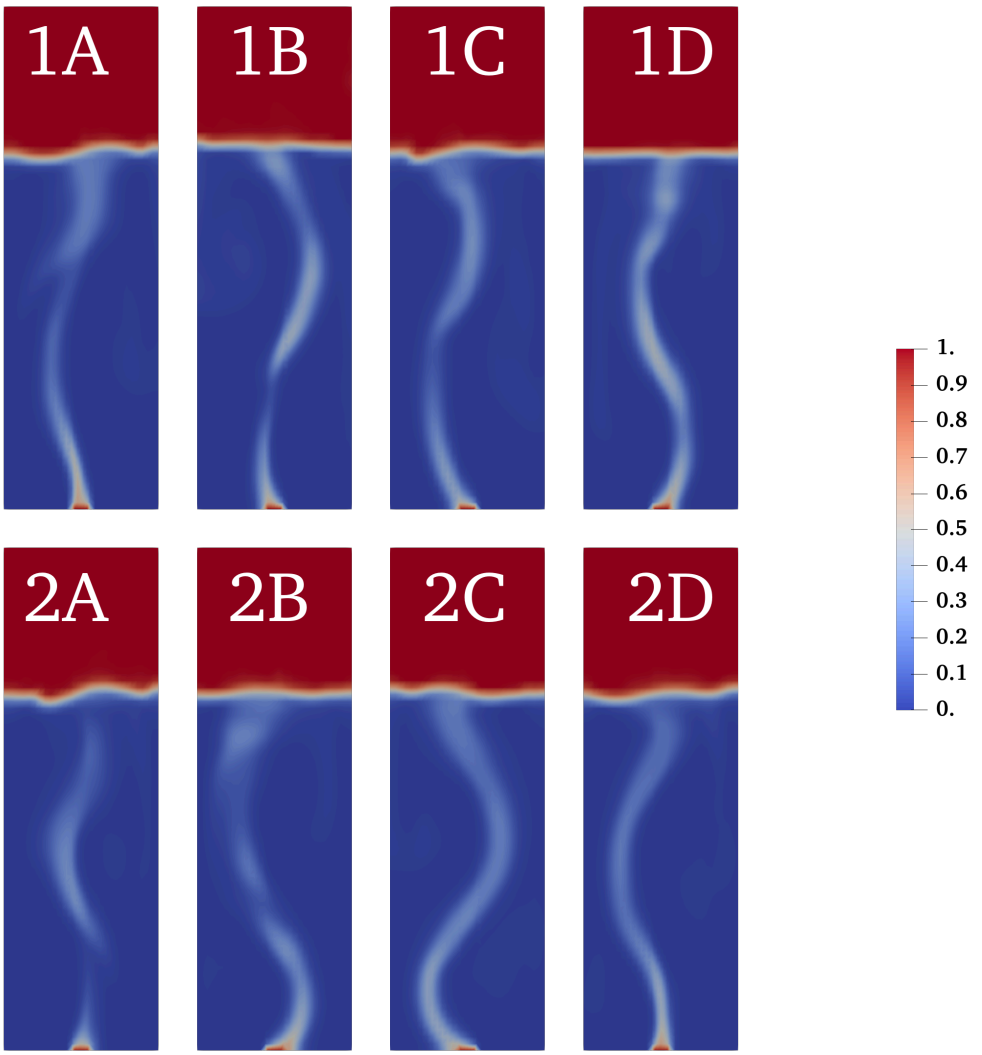

Figure 4: Instantaneous gas distributions in the different DMM implementations at gas superficial velocity is equal to 11.9 $^{mm}/_{s}$. The quantity plotted is the local gas volume fraction.

80 s, depending on the superficial velocity.

The two properties examined to assess the ability of the DMM to predict the global features of a gas-liquid system are the gas phase hold-up and the Plume Oscillation Period (POP). The hold-up is the measure of the gas volume entrapped inside the liquid of the column. The POP, on the other hand, is the measure of the time required for the plume to complete a full oscillation and corresponds to the time interval in which the horizontal velocity, taken at a point in the centre of the column, changes sign twice. An analysis of this type is straightforward if the superficial velocity is low, but it becomes unfeasible at high gas flow rate. To circumvent this problem, we use the methodology proposed by Cachaza Gianzo (2011), where the data is converted in the frequency domain, calculating the pressure fluctuation spectra. Figures 5 and 6 show the results of this analysis obtained from a simulation with a superficial velocity of 2.4 mm/s for hold-up and POP, in which it is possible to appreciate the initial transient phase which is not considered in the data analysis. The result of the pressure oscillation spectrum analysis can be seen in Fig. 7.

Table 3 presents the results obtained for all the combinations of superficial velocities, turbulence models and simplifications. DMM is particularly effective in the estimation of gas hold-up. The data obtained is, in general, very close to TFM predictions, in turn close to the experimental data. Similarly to the TFM, the DMM is closer to the experimental results for low and high velocities, resulting in less accurate predictions for intermediate values (i.e 7.1 mm/s e 11.9 mm/s), where the regime is transitional. Furthermore, there is no significant difference between the two turbulence models and the various models in term of gas hold-up. In fact, with the exception of the case at 2.4 mm/s, where models D and C are closer to the experimental data, in the others, there are no considerable differences. Noticing this, if the hold-up is the quantity investigated, the turbulence is captured slightly better by approach 2, namely the mixture turbulence model.

In Tab. 4 the computational costs of all the cases tested for the superficial velocity of 2.4 mm/s are reported and compared. It is evident that the simulations of type 2 are faster than the corresponding ones of type 1, especially for cases B and D, in which the computational cost goes up considerably. The increase in computational time of these last two simulations is a consequence of the structure of Eq. (40). As mentioned in Section 2.3, taking into account all the terms in the equation, we introduce variables that depends on $\mathbf{U}_1$, in turn dependent on $\mathbf{U}_\mathrm{r}$, the solution of the equation itself. This brings to an iterative solution of the equation each timestep, slowing the code considerably. The further increase of computational time of models 1.B and 1.D is caused by the fact that τ_{T2} is recomputed at

Superf. vel. (mm/s)	**Model type**	**Hold-up** (%)	**POP** (s)	**Exp Hold-up** (%)	**Exp POP** (s)	**Bubble diameter** (mm)
2.4	TFM	0.62	10.17	0.69	11.37	6.83
	1.A	0.62	10.38			
	2.A	0.62	12.22			
	1.B	0.67	11.58			
	2.B	0.62	10.52			
	1.C	0.62	10.24			
	2.C	0.61	9.77			
	1.D	0.68	11.88			
	2.D	0.64	10.38			
7.1	TFM	1.49	7.56	1.81	5.69	7.05
	1.A	1.43	8.35			
	2.A	1.42	9.00			
	1.B	1.45	9.36			
	2.B	1.43	8.09			
	1.C	1.41	7.89			
	2.C	1.41	8.8			
	1.D	1.43	9.22			
	2.D	1.41	8.00			
11.9	TFM	2.27	5.83	2.63	4.27	6.50
	1.A	2.14	6.02			
	2.A	2.17	6.44			
	1.B	2.25	7.37			
	2.B	2.19	6.88			
	1.C	2.16	6.97			
	2.C	2.20	5.81			
	1.D	2.40	8.10			
	2.D	2.18	6.28			
16.6	TFM	3.20	3.93	3.36	3.01	6.40
	1.A	2.88	5.39			
	2.A	3.03	5.03			
	1.B	2.66	5.82			
	2.B	2.97	6.20			
	1.C	2.90	4.49			
	2.C	2.98	4.73			
	1.D	2.69	6.38			
	2.D	2.98	4.86			
21.3	TFM	4.06	3.20	4.10	2.84	7.73
	1.A	4.08	4.00			
	2.A	4.14	4.09			
	1.B	4.47	5.71			
	2.B	4.09	4.39			
	1.C	4.10	4.49			
	2.C	4.13	4.24			
	1.D	4.45	6.29			
	2.D	4.08	4.33			

Table 3: Comparison between the results obtained for the bubble column test case for the gas volume fraction (hold-up) and the POP at different inlet superficial gas velocities with different approaches to describe turbulence and different simplifications. The label "Exp" refers to experimental data, whereas "TFM" to results obtained with the TFM; options "1" and "2" refer to the results obtained with the DMM solving respectively the k-ϵ equations with the continuous phase velocity and the mixture velocity. The last column reports the bubble diameters employed in the DMM simulation for each superficial velocity. With A we label predictions obtained with the DMM with the simplification proposed in section 2.1 and 2.3, with B no simplifications are used, with C DMM predictions are obtained with the simplification presented in 2.1 while with D those made in 2.3.

Test Case	Computational time (hh:mm:ss)
TFM 1 s	617.7 s
2.A 1 s	315.43 s
1.A	04:35:35
2.A	03:41:24
1.B	13:57:36
2.B	09:38:24
1.C	04:18:27
2.C	04:37:48
1.D	13:14:08
2.D	06:30:37

Table 4: Comparison between the computational costs of the different solvers. Top two rows: comparison between computational times for the TFM and the fastest DMM solver (2.A) evaluated by using one core of the processor i7-8550U 1.80 GHz and the same timestep of 0.001 s to simulate 1 s. Subsequent rows: computational time necessary to each DMM solver to complete the whole simulation on 10 cores of a Intel Xeon E5-2680 v3 2.50 GHz by using the same time step of 0.001 s.

each iteration, leading to the solution of the k-ϵ equation for a number of times equal to the number of the iterations done. This does not happen with τ_{Tm}, that is computed once at every time step, since $\mathbf{U}_{\mathrm{m}}$ does not depend directly on $\mathbf{U}_{\mathrm{r}}$. For these reasons, the turbulence approach 1 leads to slightly higher computational costs for A and C, but turns out to be much more expensive for B and D. Finally, from Tab. 4 it is also possible to observe the cheaper computational cost of models A and C of the DMM with respect to the TFM, confirming one of the main advantages of DMM over TFM, since DMM is about twice as fast. On the contrary, models B and D are quite slow and their computational cost may be even larger than that of the TFM.

The results concerning the POP show bigger differences than for the gas holdup. In general, the results are not far from those obtained with the TFM, but a mismatch is always present, the POPs predicted by DMM being normally from 10 to 20 % higher than those calculated by TFM. Option 1.A gave the best results, but also all models of type 2 were in good agreement with the experiments and the TFM at all the superficial velocities. The largest deviation from the TFM occurs with models 1.B and 1.D. This deterioration could be caused by the method adopted for the solution of Eq. (40), where the interdependence of the different terms makes the resolution of this equation tricky, probably leading to inaccura-

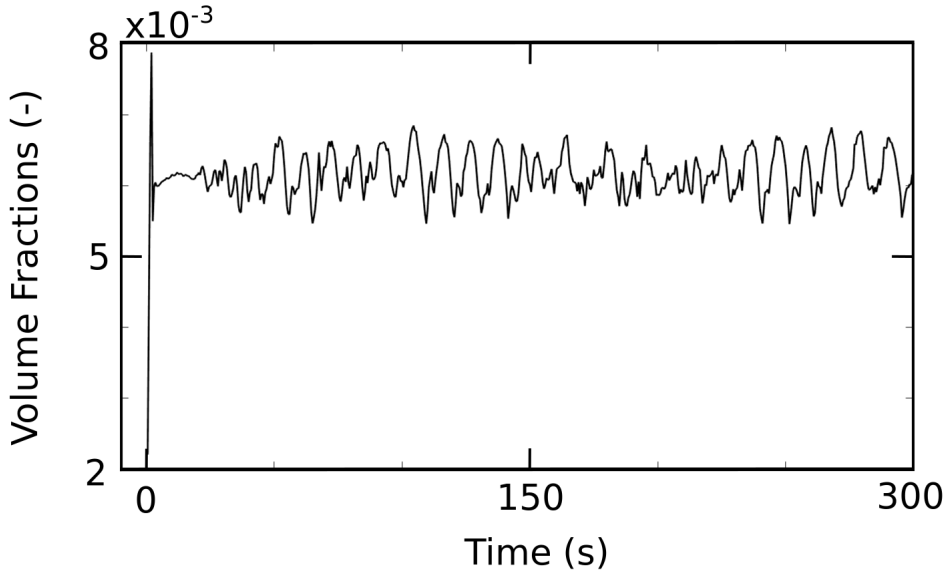

Figure 5: Time evolution of the gas volume fraction for a superficial gas velocity of 2.4 $^{mm}/_{s}$ obtained with the DMM 1.A. The initial peak is caused by the choice of the box for the evaluation. The top of the computational box is set clese to the interface between liquid and air during the simulation and in the first part of the simulation the plume creates a depression in the interface and the gas volume fraction reaches a maximum. The oscillation of the plume and the consequent entrapment of gas under the free surface bring the gas volume fraction to oscillate near the average value reported in Tab. 3. REPORT THE VOLUME FRACTION % AS IN THE OTHER PLOT.

cies in the solution process. It would, therefore, be necessary to study and implement a more accurate solution method. Indeed, a procedure such as the one used in this study, based on a Newton-Raphson method for the computation of $\mathbf{U}_r$, implemented for the interdependence of C_D from $\mathbf{U}_r$, and on consecutive reiteration for the other interdependent terms, can be further improved in the future. These deviations from the TFM prediction are more evident in 1.B and 1.D because in these cases the terms dependent from $\mathbf{U}_1$ are added to those from $\mathbf{U}_2$, on which an important term such τ_{T2} depends. To improve the performance in this part, in the future it might be useful to implement a better numerical method to compute $\mathbf{U}_r$. Last but not least, it is important to remember that $\mathbf{U}_2$ is a vector field that is not calculated from the appropriate balance equation, an aspect that, as observed in section 2.4, may lead to inaccuracies.

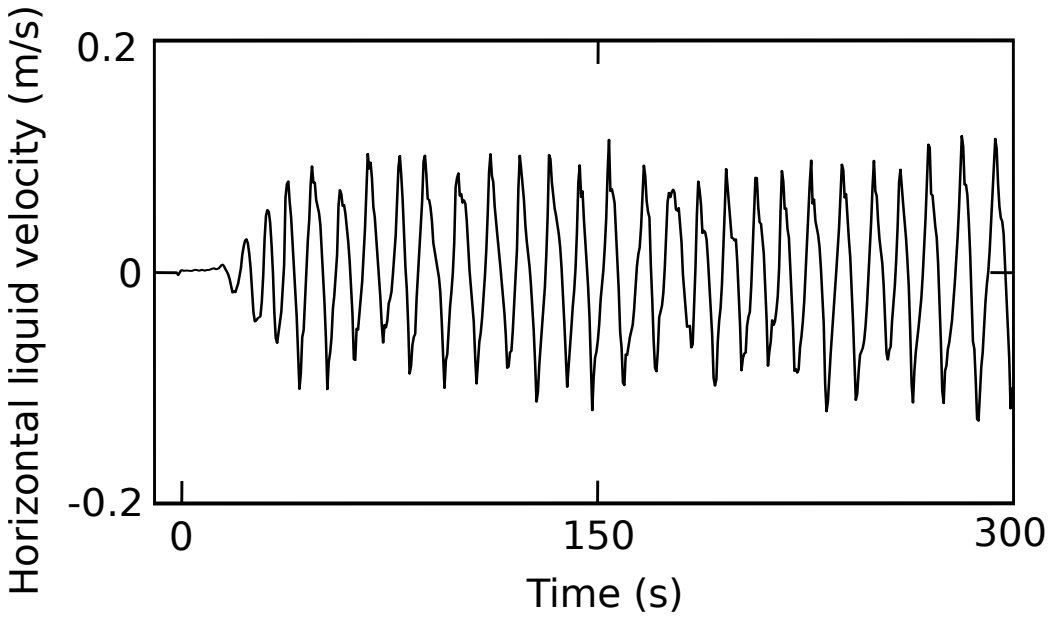

Figure 6: Time evolution of the horizontal liquid velocity for a superficial gas velocity of 2.4 $^{mm}/_{s}$ obtained with DMM 1.A. The POP is computed as the time it takes for the plume to complete an oscillation and in the plot this is the time measured between two consecutive peaks.

Both in options 1 and 2 the addition of the terms of the C model leads to an acceleration of the plume for low gas velocity and a slight slowdown for high velocity. This contrasting effect is justified by the fact that, at low velocity, the viscous term acts almost exclusively on the vertical component of the flow, in agreement with the upward motion of the bubbles, and this gives stability to the plume that is forced to oscillate along the longitudinal direction of the column. Vice-versa, high surface velocities generate a significant viscous term also in the lateral directions, inducing slight oscillation components also in the other directions, and this entails a slowing down of the plume, as the plume has to take a longer path before it returns to the initial position. In this respect the C models should be more accurate in comparison to A and B, since they do not neglect any term of the viscous stress, but apparently they overestimate this type of stress. An oscillation in the transverse direction is in fact observed also in the TFM and in the experimental data, but to a lesser extent.

For the D cases, it can be seen that they lead to good results when option 2 is adopted. We now expect that adding the C-contribution to the D model, and thus obtaining model B, a trend similar to that obtained when passing from A to

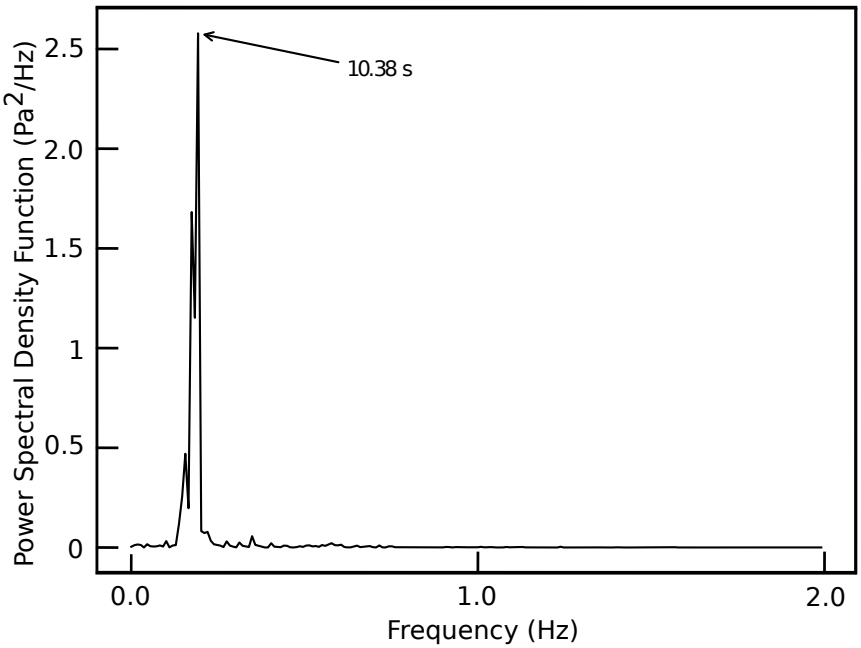

Figure 7: Power spectrum of the pressure signal for a superficial velocity of 2.4 $^{mm}/_{s}$ obtained with DMM 1.A. This alternative way to compute the POP is necessary for high superficial velocities.

C would be observed. This does not happen, probably for the same reasons that lead to unclear results in the case in which too many interdependent terms were added in the simulations (i.e. option 1), since, in the B cases, τ_m depends directly on $\mathbf{U}_r$, given that $\mathbf{U}_{M1}$ and $\mathbf{U}_{M2}$ depends on it.

In Fig. 8 and 9 the predictions for hold-up and POP obtained with DMM 1.A and 2.D are plotted. These are the most accurate in terms of hold-up and POP. For validation and benchmark these predictions are compared with results obtained with the TFM and with experiments. As it is seen DMM predictions are quite close to experiments and TFM predictions.

Figure 10 shows the vertical velocity component at three different column heights, as predicted with DMM, TFM and as measured in the experiments by Pfleger et al. (1999). As it is seen DMM predictions are in good agreement with experiments, showing once more that the is capable of also estimating local properties, such as velocity profiles. The trends obtained agree with those of TFM and

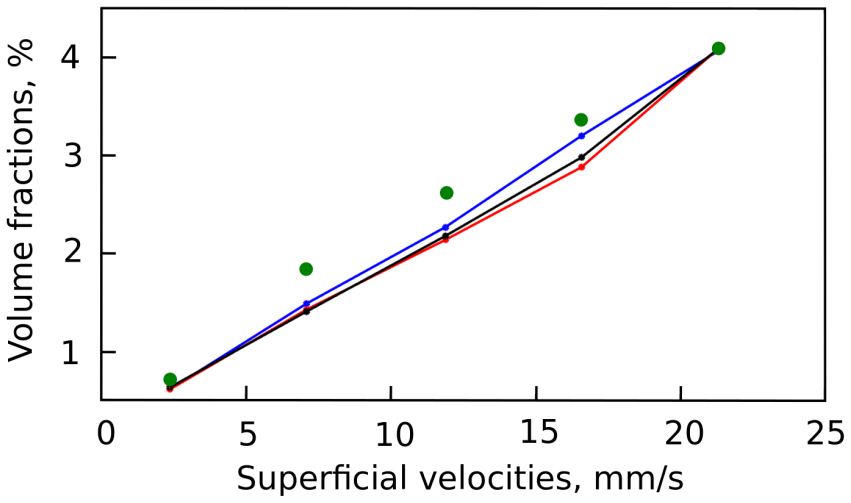

Figure 8: Comparison between global gas hold-up at different superficial velocities as measured by experiments (green circles) and predicted by the TFM (blue line) and DMM for options 1.A (red line) and 2.D (black line).

experiments, but it is clear that the predictions of the DMM with option 1 are qualitatively less accurate than those obtained with option 2. In both cases the DMM overestimates the velocities in the outer part of the column, giving instead better prediction of the velocity in the central region. The quality of the simulation is worse in the cases run with option 1, where a spurious peak is always observed in the central zone of the column. The peak is generated because in the central zone we have , on a time average basis during the whole simulation, the highest concentration of the disperse phase. This causes a lower production of turbulence, which, in option 1, is directly proportional to the fraction of the continuous phase. This effect does not occur in the simulations run with option 2, where turbulence is generated and transported by the mixture and not by a single phase. Results obtained with this option are therefore affected by higher turbulent viscosity, which make the maximum of the velocity profile less pronounced.

The deviations of the model from experiments, in all the tests performed, are, as expected, greater at the bottom of the column, since the deviations are accentuated by the proximity of the sparger, whose characteristics are the result of modeling assumptions that introduce errors. In all cases run with option 2, there are no significant differences caused by the various simplifications. This confirms

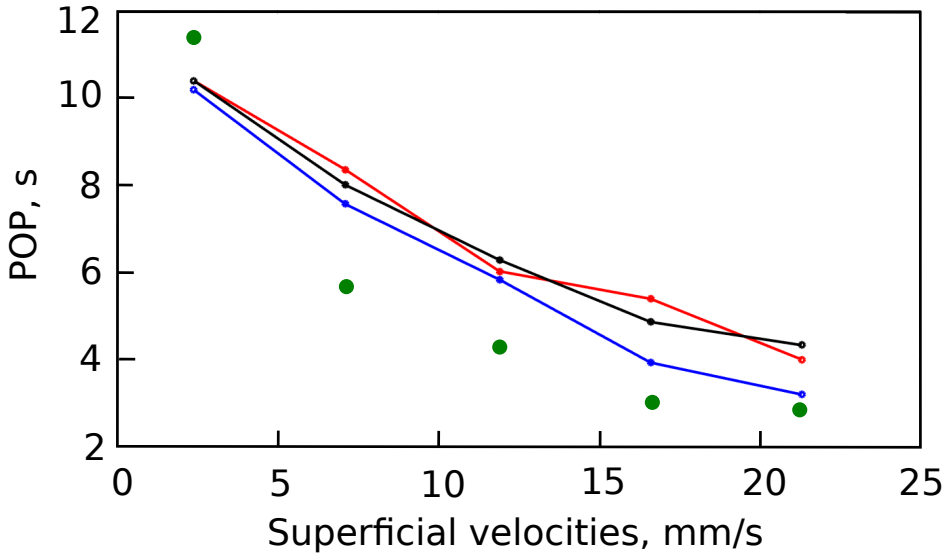

Figure 9: Comparison between POP at different superficial velocities as measured by experiments (green circles) and predicted by the TFM (blue line) and DMM for options 1.A (red line) and 2.D (black line).

the good quality of these models also for the estimation of the local properties.

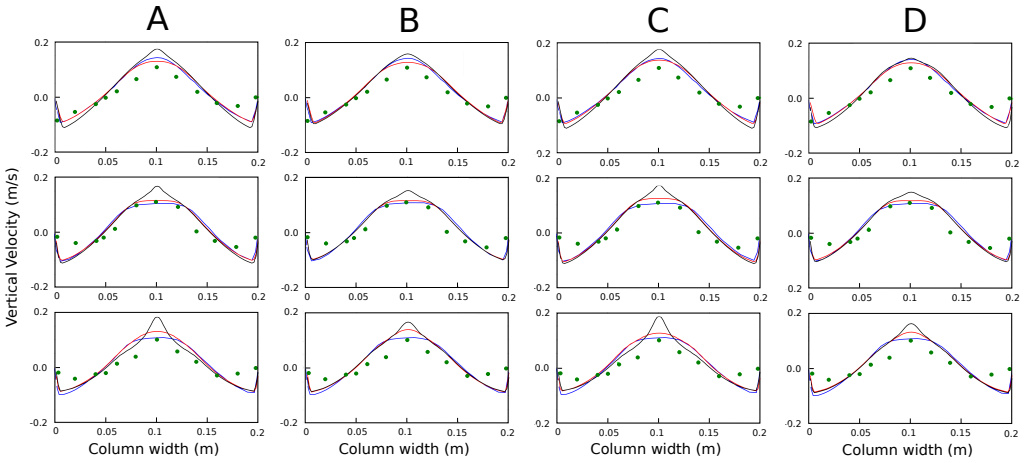

Figure 10: Comparison between experimental data, TFM and DMM at three different heights of the column studied by Pfleger and coworkers (from top to bottom: 0.37 cm - 0.25 cm - 0.13 cm). From left to right simulations obtained with the different simplifications are reported (A, B, C and D, respectively). The green circles represent the experimental data, whereas blue, black and red lines are the predictions obtained with TFM and DMM with options 1 and 2, respectively. WHAT SUPERFICIAL VELOCITY?

5. Conclusions

In this study, the Diffusion Mixture Model for gas-liquid bubbly flows has been implemented and tested in the simulation of a rectangular bubble column. In addition to the comparison with the results obtained with the TFM and experiments, a numerical investigation was conducted to verify the performance of the model when various simplifications are applied for the expression of the stress tensor and the gas-liquid relative velocity, as summarised in Tab. 3. In general, the DMM has proven to be a valid tool for modeling complex systems for which usually more accurate but computationally onerous models, such as TFM, are employed. It was shown that it is possible to treat the turbulence either as if it was generated only by the continuous phase or by the mixture phase. The first approach, similar to the one often used in the TFM, provides satisfactory results for global properties, but relatively poor predictions for local variables, such as the vertical liquid velocity along the column. On the contrary, when the turbulence is treated as a mixture property, DMM predictions result in good agreement with experiments and TFM simulations both at local and global level. In addition, fot this case of turbulence generated by the mixture, the effect of the examined simplifications on the prediction of the model was found to be minor. Consequently,

the simplest and computationally fastest form of the DMM (version A in Tab. 3) can be conveniently adopted.

Acknowledgments

This work has been financially supported by Sidel spa (Parma, Italy) in collaboration with Optimad Engineering srl (Torino, Italy).

Bibliography

Agarwal, B., Narayanan, C., 2018. Modeling of bubble flows in vertical pipes with the n-phase compressible algebraic slip model. International Journal of Multiphase Flow 105, 250–263.

Boccardo, G., Buffo, A., Marchisio, D., 2019a. Simulation of mixing in structured fluids with dissipative particle dynamics and validation with experimental data. Chemical Engineering and Technology 42 (8), 1654–1662.

Boccardo, G., Crevacore, E., Passalacqua, A., Icardi, M., 2020. Computational analysis of transport in three-dimensional heterogeneous materials: An openfoam®-based simulation framework. Computing and Visualization in Science 23 (1-4).

Boccardo, G., Crevacore, E., Sethi, R., Icardi, M., 2018a. A robust upscaling of the effective particle deposition rate in porous media. Journal of Contaminant Hydrology 212, 3–13.

Boccardo, G., Sethi, R., Marchisio, D., 2019b. Fine and ultrafine particle deposition in packed-bed catalytic reactors. Chemical Engineering Science 198, 290–304.

Boccardo, G., Sokolov, I., Paster, A., 2018b. An improved scheme for a robin boundary condition in discrete-time random walk algorithms. Journal of Computational Physics 374, 1152–1165.

Brennan, M., 2003. Multiphase CFD simulations of dense medium and classifying hydrocyclones. Third International Conference on CFD in the Minerals and Process Industries, Melbourne, Australia.

Buffo, A., Marchisio, D., 2014. Modeling and simulation of turbulent polydisperse gas-liquid systems via the generalized population balance equation. Reviews in Chemical Engineering 30 (1), 73–126.

Buffo, A., Marchisio, D. L., Vanni, M., Renze, P., 2013a. Simulation of polydisperse multiphase systems using population balances and example application to bubbly flows. Chemical Engineering Research and Design 91, 1859–1875.

Buffo, A., Vanni, M., Marchisio, D., 2012. Multidimensional population balance model for the simulation of turbulent gas-liquid systems in stirred tank reactors. Chemical Engineering Science 70, 31–44.

Buffo, A., Vanni, M., Marchisio, D., 2017. Simulation of a reacting gas-liquid bubbly flow with cfd and pbm: Validation with experiments. Applied Mathematical Modelling 44, 43–60.

Buffo, A., Vanni, M., Marchisio, D., Fox, R., 2013b. Multivariate quadrature-based moments methods for turbulent polydisperse gas-liquid systems. International Journal of Multiphase Flow 50, 41–57.

Buffo, A., Vanni, M., Renze, P., Marchisio, D., 2016. Empirical drag closure for polydisperse gas-liquid systems in bubbly flow regime: Bubble swarm and micro-scale turbulence. Chemical Engineering Research and Design 113, 284–303.

Cachaza Gianzo, E. M., Jun. 2011. Hydrodynamics and mass transfer effects in bubble columns. Ph. D. Thesis, Universidad de Salamanca, Salamanca, Spain.

Chen, P., Sanyal, J., Dudukovic, M. P., 2004. Cfd modeling of bubble columns flows: implementation of population balance. Chemical Engineering Science 59, 5201–5207.

Crevacore, E., Boccardo, G., Grillo, A., Marchisio, D., Sethi, R., 2017. Pore-scale simulations of particle transport for groundwater remediation: The effect of gravitational settling. Chemical Engineering Transactions 60, 193–198.

Crevacore, E., Boccardo, G., Marchisio, D., Sethi, R., 2016. Microscale colloidal transport simulations for groundwater remediation. Chemical Engineering Transactions 47, 271–276.

Diaz, M. E., Montes, F. J., Galan, M. A., 2008. Experimental study of the transition between unsteady flow regimes in a partially aerated two-dimensional bubble column. Chemical Engineering and Processing 47, 1867–1876.

Frank, T., Zwart, P., Krepper, E., Prasser, H. M., Lucas, D., 2008. Validation of cfd models for mono- and polydisperse air-water two-phase flows in pipes. Nuclear Engineering and Design 238, 647–659.

Frungieri, G., Boccardo, G., Buffo, A., Marchisio, D., Karimi-Varzaneh, H., Vanni, M., 2020. A cfd-dem approach to study the breakup of fractal agglomerates in an internal mixer. Canadian Journal of Chemical Engineering.

Gemello, L., Cappello, V., Augier, F., Marchisio, D., Plais, C., 2018a. Cfd-based scale-up of hydrodynamics and mixing in bubble columns. Chemical Engineering Research and Design 136, 846–858.

Gemello, L., Plais, C., Augier, F., Cloupet, A., Marchisio, D., 2018b. Hydrodynamics and bubble size in bubble columns: Effects of contaminants and sparggers. Chemical Engineering Science 184, 93–102.

Gemello, L., Plais, C., Augier, F., Marchisio, D., 2019. Population balance modelling of bubble columns under the heterogeneous flow regime. Chemical Engineering Journal 372, 590–604.

Goda, H., Hibiki, T., Kim, S., Ishii, M., Uhle, J., 2003. Drift-flux model for downward two-phase flow. International Journal of Heat and Mass Transfer 46, 4853–4844.

Hager, A., Kloss, C., Pirker, S., Goniva, C., 2013. Parallel resolved open source CFD-DEM: method. The Journal of Computational Multiphase Flows 6, 13–27.

Hermann, M., 2010. A parallel eulerian interface tracking/lagrangian point particle multi-scale coupling procedure. Journal of Computational Physics 229, 745–759.

Hibiki, T., Ishii, M., 2003a. One-dimensional drift-flux model and constitutive equations for relative motion between phases in various two-phase flow regimes. International Journal of Heat and Mass trasnfer 46, 4935–4948.

Hibiki, T., Ishii, M., 2003b. One-dimensional drift-flux model for two-phase flow in a large diameter pipe. International Journal of Heat and Mass Transfer 46, 1773–1790.

Hirt, C. W., Nichols, B. D., 1981. Volume of fluid (vof) method for the dynamics of free boundaries. Journal of Computational Physics 39, 201–225.

Horsch, M., Niethammer, C., Boccardo, G., Carbone, P., Chiacchiera, S., Chiricotto, M., Elliott, J., Lobaskin, V., Neumann, P., Schiffels, P., Seaton, M., Todorov, I., Vrabec, J., Cavalcanti, W., 2020. Semantic interoperability and characterization of data provenance in computational molecular engineering. Journal of Chemical and Engineering Data 65 (3), 1313–1329.

Icardi, M., Boccardo, G., Tempone, R., 2016. On the predictivity of pore-scale simulations: Estimating uncertainties with multilevel monte carlo. Advances in Water Resources 95, 46–60.

Icardi, M., Marchisio, D., Chidambaram, N., Fox, R., 2013. Equilibrium-eulerian les model for turbulent poly-dispersed particle-laden flow. International Journal of Nonlinear Sciences and Numerical Simulation 14 (2), 139–158.

Icardi, M., Ronco, G., Marchisio, D., Labois, M., 2014. Efficient simulation of gas-liquid pipe flows using a generalized population balance equation coupled with the algebraic slip model. Applied Mathematical Modelling 38 (17-18), 4277–4290.

Ishii, M., Mishima, K., 1984. Two-fluid model and hydrodynamic constitutive relations. Nuclear Engineering and Design 82, 107–126.

Manninen, M., Taivassalo, V., 1996. On the mixture model for multiphase flow. VTT Technical Publications, 288, ESPOO Finland.

Marcato, A., Boccardo, G., Marchisio, D., 2020. A computational workflow to study particle transport in porous media: Coupling cfd and deep learning. Computer Aided Chemical Engineering 48, 1759–1764.

Marchisio, D. L., Fox, R. O., 2013. Computational Models for Polydisperse Particulate and Multiphase Systems. Cambridge University Press, Cambridge, UK.

Narasimha, M., Brenna, M., Holtham, P. N., 2007. A review of CFD modelling for performance predictions of hydrocyclone. Engineering Applications of Computational Fluid Mechanics 1, 109–125.

Pfleger, D., Gomes, S., Gilbert, N., Wagner, H. G., 1999. Hydrodynamic simulations of laboratory scale bubble columns fundamental studies of the eulerian-eulerian modelling approach. Chemical Engineering Science 54, 5091–5099.

Pham, T. Q. D., Jeon, J., Choi, S., 2020. Quantitative comparison between volume-of-fluid and two-fluid models for two-phase flow simulation using openfoam. Journal of Mechanical Science and Technology 34, 1157–1166.

Press, W. H., Teukolsky, S. A., Vetterling, W. T., P., F. B., 2007. Numerical Recipes: The Art of Scientific Computing. Cambridge University Press, Cambridge, UK.

Renze, P., Buffo, A., Marchisio, D., Vanni, M., 2014. Simulation of coalescence, breakup, and mass transfer in polydisperse multiphase flows. Chemie-Ingenieur-Technik 86 (7), 1088–1098.

Rielly, C., Marquis, A., 2001. A particles's eye view of crystallizer fluid mechanics. Chemical Engineering Science 56, 2475–2493.

Shiea, M., Buffo, A., Baglietto, E., Lucas, D., Vanni, M., Marchisio, D., 2019. Evaluation of hydrodynamic closures for bubbly regime cfd simulations in developing pipe flow. Chemical Engineering and Technology 42 (8), 1618–1626.

Tabib, M. V., Roy, S. A., Joshi, J. B., 2007. Cfd simulation of bubble column - an analysis of interphase forces and turbulence models. Chemical Engineering Journal 139, 589–614.

Tomiyama, A., Celata, G. P., Hosokawa, S., Yoshida, S., 2002. Terminal velocity of single bubbles in surface tension force dominant regime. International Journal of Multiphase Flow 28, 1497–1519.

Ungarish, M., 1993. Hydrodynamics of suspensions: Fundamentals of centrifugal and gravity separation. Springer.